actuators

MDPI

Article

Integrated Adaptive Sliding Mode-Based Control and Disturbance Observer for Robot Manipulators Under Actuator Saturation

Sion Lee, Yuna Hong and Jaeyoung Kang *

Department of Mechanical Engineering, Inha University, 100 Inha-ro, Michuhol-gu, Incheon 22212, Republic of Korea; sion.lee@inha.edu (S.L.); hyun99@inha.edu (Y.H.)
* Correspondence: kangj@inha.ac.kr

Abstract

This paper presents an adaptive control framework that unifies control and observation for robotic manipulators under actuator saturation and dynamic uncertainties. An Input-Constrained Adaptive Sliding Mode Controller (ICASMC) is integrated with an Adaptive Sliding Mode Disturbance Observer (ASMDOB) through a shared adaptive law that simultaneously compensates for saturation-induced transient degradation and initial observer estimation delay. This unified adaptive structure enables faster disturbance convergence and improved transient response without conservative bounds. Under the stated assumptions, the Lyapunov analysis establishes the boundedness of the closed-loop signals. The proposed framework is evaluated through numerical simulations of a planar spacecraft–manipulator system and experiments on a ground-based three-degree-of-freedom manipulator. The experimental results show lower tracking errors than those obtained with a sliding mode control (SMC) comparator and a PID controller under the same actuator limits, while maintaining relatively smooth control inputs.

Keywords: robotic manipulators; actuator saturation; adaptive sliding mode control; disturbance observer; robust control

1. Introduction

Robotic manipulators are widely employed in real-world applications, but their control performance is challenged by uncertainties such as unmodeled dynamics, parameter drift, and external disturbances. These difficulties are further aggravated by actuator saturation arising from physical torque or velocity limits, which can cause large tracking errors or even instability in closed-loop systems [1–3]. Owing to nonlinear dynamics and strong coupling, robotic manipulators are highly sensitive to uncertainties from payload changes, friction, and structural flexibility. Nevertheless, many existing control studies still neglect the stability implications of actuator saturation [4–7], despite its critical impact on performance and safety.

Beyond their standalone importance, manipulators integrated with mobile robotic platforms—such as UAVs, space vehicles, and ground robots—have broadened their capabilities for complex operations across aerial, terrestrial, and space environments [8]. This combination demands control strategies that are robust to inherent uncertainties and can manage dynamic coupling, environmental disturbances, and actuator limits simultaneously [9–13]. Hence, developing an integrated robust control framework that explicitly

Check for updates

Academic Editor: Xiaozheng Jin

Received: 16 September 2026
Revised: 10 November 2026
Accepted: 12 November 2026
Published: 17 November 2026

Copyright: © 2026 by the authors. Licensee MDPI, Basel, Switzerland. This article is an open access article distributed under the terms and conditions of the Creative Commons Attribution (CC BY) license.

considers actuator saturation and real-time disturbance estimation is becoming increasingly crucial.

Several classical control strategies have been extended to explicitly address actuator saturation in robotic systems. Event-triggered control (ETC) reduces control update frequency to alleviate actuator saturation [14], and optimization-based ETC-PID tuning enlarges the domain of attraction under input constraints [15]. Although easy to implement, these methods generally lack robustness to system uncertainties. Model Predictive Control (MPC) has also been investigated for systems with input constraints [16,17]. In online implementations, model mismatch can affect prediction accuracy, while solving the constrained optimization problem within the sampling interval can be computationally demanding at high sampling rates. When a disturbance observer is incorporated, the disturbance estimates need to be accounted for in the predictive control formulation, and residual estimation errors need to be considered when assessing constraint satisfaction and closed-loop stability.

The integration of Sliding Mode Control (SMC) with Barrier Lyapunov Functions (BLFs) has been studied to handle input constraints [1,18–20], providing a rigorous way to maintain system states within bounds. However, BLF-based methods have notable practical limitations. They require system states to initially lie within constrained sets, which is difficult in robotic systems under disturbances or measurement noise. Violation of this condition can cause unbounded BLF growth and instability. Furthermore, as states approach constraint boundaries, BLFs often generate rapidly increasing control effort, aggravating actuator saturation instead of preventing it.

Adaptive sliding mode control (ASMC) has been studied to address model uncertainties and bounded disturbances under input constraints [1,21]. However, accurate real-time parameter estimation remains difficult and typically requires conservative upper bounds, resulting in large adaptive gains and increased chattering. These limitations highlight the need to integrate disturbance observers (DOBs) for real-time uncertainty estimation and reduced dependence on conservative adaptation.

In parallel, Disturbance Observer (DOB) theory has become a key approach for robust motion control, enabling estimation and compensation of external disturbances and model uncertainties in real time [22,23]. An adaptive sliding mode disturbance observer was developed without requiring prior knowledge of the bound on the time derivative of the system uncertainty [24]. The observer was combined with a controller designed to achieve prescribed transient and steady-state tracking performance. However, eliminating the need for this uncertainty bound does not by itself ensure that the prescribed tracking performance is maintained when actuator saturation alters the commanded control input. The interaction between disturbance estimation and input constraints must therefore also be considered in the controller–observer design. Backstepping-based adaptive sliding mode DOBs have also been proposed [25], where a virtual system is used to reproduce plant dynamics and improve disturbance rejection. Yet, their performance strongly relies on accurately designed virtual states and auxiliary variables, which increase implementation complexity. Furthermore, the backstepping structure adds computational burden from auxiliary variable and adaptive gain updates, limiting real-time applicability in resource-constrained systems.

Several studies have proposed robust control frameworks to address actuator saturation [26–29], offering strategies to maintain stability and performance under input limits. Adaptive neural control and observer-based control have also been investigated for systems with actuator constraints [30–34]. In [32], a neural state observer was combined with actuator-saturation compensation, and the tracking errors were shown to converge to bounded regions within finite time. In [33], a nonlinear state observer was incorporated into an adaptive optimized output-feedback controller for stochastic nonlinear systems with input and state constraints, ensuring boundedness of the closed-loop signals. The observers

in these two studies reconstruct unmeasured states, which differs from directly estimating lumped disturbances for control compensation.

Disturbance estimation has also been incorporated into control systems subject to actuator saturation. Pan et al. [34] combined adaptive robust control with a terminal sliding-mode disturbance observer and established finite-time convergence of the disturbance estimation error. However, the observer switching gain depends on a prescribed bound on the time derivative of the lumped disturbance. This requirement motivates the use of online uncertainty information in observer-gain adjustment. For the present application, particular attention is given to the initial estimation transient, during which residual disturbance-estimation errors and actuator saturation can jointly affect tracking performance. To address this issue, this paper presents an integrated ICASMC–ASMDOB framework in which the uncertainty-bound estimate obtained by the controller is incorporated into the observer switching gain. This sharing of adaptive information is intended to improve transient disturbance estimation and tracking under actuator saturation.

Table 1 summarizes the main features of representative control approaches.

Table 1. Comparison of existing control approaches and the proposed method.

Ref.	Saturation	DOB	Conservative Assumptions	Optimization
[1]	O	X	X	X
[14]	O	X	O	O
[16]	O	X	O	O
[21]	O	X	X	X
[24]	X	O	O	X
[25]	X	O	X	X
[32]	O	X	X	X
[34]	O	O	O	X
Proposed	O	O	X	X

O: yes; X: no. Conservative assumptions denote a priori known bounds on model uncertainties or uncertain model parameters. Optimization indicates explicit numerical optimization, rather than measured computational cost.

The main contributions of this work are as follows:

(1) A unified adaptive control framework is developed to handle actuator saturation and dynamic uncertainties, where all unknown bounds of multiple uncertainty terms are adaptively estimated in real time without requiring a priori numerical values of the uncertainty bounds estimated by the adaptive laws.
(2) A cross-coupled adaptive mechanism is introduced, injecting the uncertainty bound estimated by the ICASMC into the ASMDOB's switching gain to enhance robustness and transient disturbance estimation.
(3) The proposed framework is evaluated through numerical simulations of a planar spacecraft–manipulator system and experiments on a fixed-base three-degree-of-freedom manipulator. The experimental comparison quantifies tracking accuracy and actuator saturation using total RMSE, cumulative saturation duration, and saturation event counts.

The remainder of this paper is organized as follows. Section 2 presents the system model and problem formulation, followed by the design of the Input-Constrained Adaptive Sliding Mode Controller (ICASMC). Section 3 develops the Adaptive Sliding Mode Disturbance Observer (ASMDOB) and describes its integration with the controller. Section 4 presents the numerical simulation and experimental results. Section 5 discusses the findings and concludes the paper. The main symbols and abbreviations are summarized in Appendix A.

2. System Modeling and Problem Formulation

2.1. Dynamic Modeling of Robot Manipulator

The dynamic model of an n-DOF robot manipulator can be described by the following standard form:

$$\mathbf{M}_o(\mathbf{q})\ddot{\mathbf{q}} + \mathbf{C}_o(\mathbf{q}, \dot{\mathbf{q}})\dot{\mathbf{q}} + \mathbf{G}_o(\mathbf{q}) = \boldsymbol{\tau} + \mathbf{d}_l \tag{1}$$

Here, $\mathbf{q} \in \mathbb{R}^n$ is the joint position vector, and $\mathbf{M}_o(\mathbf{q}) \in \mathbb{R}^{n\times n}$ is the inertia matrix. The term $\mathbf{C}_o(\mathbf{q}, \dot{\mathbf{q}}) \in \mathbb{R}^{n\times n}$ denotes the Coriolis matrix, while $\mathbf{G}_o(\mathbf{q}) \in \mathbb{R}^n$ represents the gravity vector. The control input torque is given by $\boldsymbol{\tau} \in \mathbb{R}^n$. The term $\mathbf{d}_l \in \mathbb{R}^n$ represents the lumped disturbance, which encapsulates internal model uncertainties (such as parameter variations, friction, and backlash) and unknown external disturbances.

For simplicity of notation, we will write $\mathbf{M}_o$, $\mathbf{C}_o$, and $\mathbf{G}_o$ instead of $\mathbf{M}_o(\mathbf{q})$, $\mathbf{C}_o(\mathbf{q}, \dot{\mathbf{q}})$, and $\mathbf{G}_o(\mathbf{q})$, respectively.

2.2. Design of ASMC Under Actuator Saturation

This section develops the ICASMC for robust tracking under actuator saturation, in coordination with the ASMDOB presented in Section 3. As shown in Figure 1, the limited input is supplied to both the manipulator and the virtual system. The ASMDOB feeds the disturbance estimate back to the control law, while the ICASMC provides its adaptive uncertainty-bound estimate to the observer switching gain.

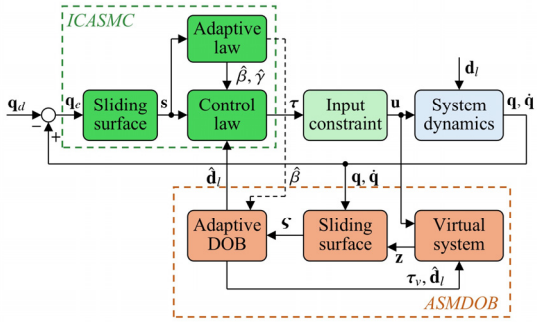


Figure 1. Signal-flow diagram of the integrated ICASMC–ASMDOB framework with actuator saturation and adaptive information sharing.

Before designing the controller, we define the saturated input $\mathbf{u}$ that is applied to the system. To do this, we must first define the saturation matrix $\boldsymbol{\Phi}(\boldsymbol{\tau})$, as follows

$$\mathbf{u} = \boldsymbol{\Phi}(\boldsymbol{\tau}) \cdot \boldsymbol{\tau} \tag{2}$$

where $\boldsymbol{\Phi}(\boldsymbol{\tau}) = \mathrm{diag}[\phi_1(\tau_1),\cdots,\phi_n(\tau_n)]$ and each τ_{mi} denotes the maximum torque limit of each actuator.

$$\phi_i(\tau_i) = \begin{cases} \tau_{mi}/|\tau_i|, & \text{if } |\tau_i| > \tau_{mi} \\ 1, & \text{otherwise} \end{cases} \tag{3}$$

Each diagonal entry of the saturation matrix represents the attenuation of the corresponding commanded input. It equals one when the input is within the actuator limit and becomes smaller than one when the command exceeds that limit. Thus, $\mathbf{u}$ represents the limited input applied to the system, whereas $\boldsymbol{\tau}$ denotes the commanded input.

The system dynamics can thus be rewritten as follows:

$$\mathbf{M}_o\ddot{\mathbf{q}} + \mathbf{C}_o\dot{\mathbf{q}} + \mathbf{G}_o = \boldsymbol{\Phi}(\boldsymbol{\tau}) \cdot \boldsymbol{\tau} + \mathbf{d}_l \tag{4}$$

Let the tracking error be defined as $\mathbf{q}_e = \mathbf{q} - \mathbf{q}_d$, and define the sliding manifold as follows:

$$\mathbf{s} = \dot{\mathbf{q}}_e + \boldsymbol{\Lambda}\mathbf{q}_e \tag{5}$$

where $\mathbf{\Lambda}$ is a positive definite diagonal gain matrix.

According to (4), the sliding mode dynamics can be obtained as follows.

$$\mathbf{M}_o\dot{\mathbf{s}} + \mathbf{C}_o\mathbf{s} = -\mathbf{M}_o\ddot{\mathbf{q}}_d - \mathbf{C}_o\dot{\mathbf{q}}_d - \mathbf{G}_o + \mathbf{M}_o\mathbf{\Lambda}\dot{\mathbf{q}}_e + \mathbf{C}_o\mathbf{\Lambda}\mathbf{q}_e + \mathbf{\Phi}(\boldsymbol{\tau})\cdot\boldsymbol{\tau} + \mathbf{d}_l \tag{6}$$

Assumption 1. *There exists a positive constant γ satisfying the following inequality, which arises from the inherent physical limitations of the system [35].*

$$0 < \gamma \leq \min\phi_i \leq 1 \tag{7}$$

Let β denote the unknown constant characterizing the uncertainty bound specified in Assumption 2 below. A hat denotes an adaptive estimate of the corresponding parameter. Accordingly, $\hat{\beta}$ and $\hat{\gamma}$ denote the adaptive estimates of β and γ, respectively. Consider the following Lyapunov function:

$$V_1 = \frac{1}{2}\mathbf{s}^T\mathbf{M}_o\mathbf{s} + \frac{1}{2}\tilde{\beta}^2 + \frac{1}{2}\tilde{\gamma}^2 \tag{8}$$

where $\sim$ denotes the estimation error (e.g., $\tilde{\beta} = \beta - \hat{\beta}$).

The time-derivative of V_1 can be obtained as

$$\begin{aligned} \dot{V}_1 &= \mathbf{s}^T\mathbf{M}_o\dot{\mathbf{s}} + \tilde{\beta}\dot{\tilde{\beta}} + \tilde{\gamma}\dot{\tilde{\gamma}} \\ &= \mathbf{s}^T\left(\mathbf{H}_{eq} + \mathbf{\Phi}(\boldsymbol{\tau})\boldsymbol{\tau}_{eq} + \mathbf{\Phi}(\boldsymbol{\tau})\boldsymbol{\tau}_r\right) + \tilde{\beta}\dot{\tilde{\beta}} + \tilde{\gamma}\dot{\tilde{\gamma}} \end{aligned} \tag{9}$$

where $\mathbf{H}_{eq}$ denotes the equivalent term that must be rejected to ensure the system trajectories remain confined to the sliding manifold.

$$\mathbf{H}_{eq} = \mathbf{M}_o(-\ddot{\mathbf{q}}_d + \mathbf{\Lambda}\dot{\mathbf{q}}_e) + \mathbf{C}_o(-\mathbf{s} - \dot{\mathbf{q}}_d + \mathbf{\Lambda}\mathbf{q}_e) - \mathbf{G}_o + \mathbf{d}_l \tag{10}$$

where $\boldsymbol{\tau}_{eq} = -\hat{\mathbf{H}}_{eq}$. In $\hat{\mathbf{H}}_{eq}$ only the disturbance term $\mathbf{d}_l$ is estimated, while the remaining terms in $\mathbf{H}_{eq}$ are assumed to be known exactly. To enhance control performance and reduce chattering, the control input is split into an equivalent term and a nonlinear rejection input, i.e., $\boldsymbol{\tau} = \boldsymbol{\tau}_{eq} + \boldsymbol{\tau}_r$.

Remark 1. *The control input $\boldsymbol{\tau}$ is divided into an equivalent term $\boldsymbol{\tau}_{eq}$ and a rejection term $\boldsymbol{\tau}_r$, primarily to enable effective integration with the DOB. The equivalent term combines the nominal model contribution with the estimated lumped disturbance. The rejection term supplements this compensation to address the residual uncertainty and the effects of actuator saturation.*

Assumption 2. *There exists a constant β that satisfies the following inequality.*

$$\left\|\mathbf{H}_{eq} + \mathbf{\Phi}(\boldsymbol{\tau})\boldsymbol{\tau}_{eq}\right\| \leq \beta\gamma^{\alpha+1} \tag{11}$$

where γ is the known constant defined in the previous assumption and $\alpha > 0$. The constant β is unknown, and its adaptive estimate obtained by the ICASMC is used in the ASMDOB to improve the observer's initial transient performance.

According to (11), $\mathbf{s}^T(\mathbf{H}_{eq} + \mathbf{\Phi}(\boldsymbol{\tau})\boldsymbol{\tau}_{eq}) \leq \beta\gamma^{\alpha+1}\|\mathbf{s}\|$ holds and is expressed as

$$\dot{V}_1 \leq \beta\gamma^{\alpha+1}\|\mathbf{s}\| + \mathbf{s}^T\mathbf{\Phi}(\boldsymbol{\tau})\boldsymbol{\tau}_r + \tilde{\beta}\dot{\tilde{\beta}} + \tilde{\gamma}\dot{\tilde{\gamma}} \tag{12}$$

Theorem 1. *For the system in (4) consider the following adaptive laws.*

$$\dot{\hat{\beta}} = \mu_1\hat{\gamma}^{\alpha+1}\|\mathbf{s}\| \tag{13}$$

$$\dot{\hat{\gamma}} = -\mu_2\hat{\beta}\hat{\gamma}^{\alpha}\|\mathbf{s}\| \tag{14}$$

where $\mu_1 > 0$ and $\mu_2 > 0$ are design parameters. Consider the nonnegative solution of the adaptive laws with $\hat{\beta}(0) > 0$, $0 < \hat{\gamma}(0) < 1$. Along any solution defined for all $t \geq 0$, the adaptive estimates converge to finite constants $\hat{\beta}_\infty$ and $\hat{\gamma}_\infty$, satisfying

$$\hat{\beta}_\infty \geq \hat{\beta}(0) \tag{15}$$

$$0 \leq \hat{\gamma}_\infty \leq \hat{\gamma}(0) \tag{16}$$

Consequently, the estimation errors converge to

$$\lim_{t\to\infty} \tilde{\beta}(t) \;=\; \beta - \hat{\beta}_\infty \tag{17}$$

$$\lim_{t\to\infty} \tilde{\gamma}(t) \;=\; \gamma - \hat{\gamma}_\infty \tag{18}$$

These limits depend on the initial estimates and the evolution of the sliding variable and are not necessarily zero.

For the subsequent closed-loop convergence analysis, additionally assume that $\gamma \leq \hat{\gamma}(t)$ holds for all $t \geq 0$.

Furthermore, consider the adaptive compensation input $\boldsymbol{\tau}_r$ given by

$$\boldsymbol{\tau}_r \;=\; -\boldsymbol{\sigma}\mathbf{s} - \mu_3\hat{\beta}(\hat{\gamma} + \lambda)^{\alpha}\frac{\mathbf{s}}{\|\mathbf{s}\|} \tag{19}$$

where $\lambda > 0$ is the compensator gain, decreasing when the DOB is reliable and increasing otherwise. $\boldsymbol{\sigma} = \mathrm{diag}[\sigma_1,\cdots,\sigma_n]$ is the control gain. As a result, the state trajectories can be driven to the sliding manifold $\lim_{t\to\infty}\mathbf{s}(t) \;=\; 0$.

Proof. We first establish the convergence of the adaptive estimates. From (13) and (14),

$$\begin{aligned} \tfrac{d}{dt}\left(\mu_2\hat{\beta}^2 + \mu_1\hat{\gamma}^2\right) &= 2\mu_2\hat{\beta}\dot{\hat{\beta}} + 2\mu_1\hat{\gamma}\dot{\hat{\gamma}} \\ &= 2\mu_1\mu_2\hat{\beta}\hat{\gamma}^{\alpha+1}\|\mathbf{s}\| - 2\mu_1\mu_2\hat{\beta}\hat{\gamma}^{\alpha+1}\|\mathbf{s}\| \\ &= 0. \end{aligned} \tag{20}$$

Thus, the weighted sum retains its initial value, and both adaptive estimates are bounded because $\mu_1 > 0$ and $\mu_2 > 0$. On the nonnegative domain specified in the theorem, $\hat{\beta}$ is nondecreasing and $\hat{\gamma}$ is nonincreasing. Therefore, along any solution defined for all $t \geq 0$, the estimates converge to finite limits. The estimation-error limits stated in (17) and (18) then follow directly from the definitions of $\tilde{\beta}$ and $\tilde{\gamma}$.

We next consider the time derivative of the Lyapunov function V_1. Since β and γ are constants, the estimation-error definitions give $\dot{\tilde{\beta}} \;=\; -\dot{\hat{\beta}}$ and $\dot{\tilde{\gamma}} \;=\; -\dot{\hat{\gamma}}$, respectively. The following estimate uses the additional condition $\gamma \leq \hat{\gamma}(t)$. Since $\alpha > 0$, this condition implies $\gamma^{\alpha+1} \leq \hat{\gamma}^{\alpha+1}$.

$$\begin{aligned} \dot{V}_1 &\leq \beta\hat{\gamma}^{\alpha+1}\|\mathbf{s}\| - \mu_1\beta\hat{\gamma}^{\alpha+1}\|\mathbf{s}\| + \mu_1\hat{\beta}\hat{\gamma}^{\alpha+1}\|\mathbf{s}\| + \mu_2\gamma\hat{\gamma}^{\alpha}\hat{\beta}\|\mathbf{s}\| - \mu_2\hat{\gamma}^{\alpha+1}\hat{\beta}\|\mathbf{s}\| + \mathbf{s}^T\boldsymbol{\Phi}(\boldsymbol{\tau})\boldsymbol{\tau}_r \\ &= (1-\mu_1)\beta\hat{\gamma}^{\alpha+1}\|\mathbf{s}\| + (\mu_1-\mu_2)\hat{\beta}\hat{\gamma}^{\alpha+1}\|\mathbf{s}\| + \mu_2\gamma\hat{\gamma}^{\alpha}\hat{\beta}\|\mathbf{s}\| - \sum_{i=1}^{n}\phi_i\sigma_i s_i^2 - \mu_3\hat{\beta}(\hat{\gamma}+\lambda)^{\alpha}\sum_{i=1}^{n}\phi_i\|\mathbf{s}\| \end{aligned} \tag{21}$$

Here, the condition $1 < \mu_1 < \mu_2$ is imposed and based on the relationship in (7), the following inequality is derived.

$$\begin{aligned} \dot{V}_1 &\leq \mu_2\gamma\hat{\gamma}^{\alpha}\hat{\beta}\|\mathbf{s}\| - \mu_3\hat{\beta}(\hat{\gamma}+\lambda)^{\alpha}(\min\phi_i)\|\mathbf{s}\| \\ &\leq \mu_2\gamma\hat{\gamma}^{\alpha}\hat{\beta}\|\mathbf{s}\| - \mu_3\hat{\beta}(\hat{\gamma}+\lambda)^{\alpha}\gamma\|\mathbf{s}\| \\ &= \left(\mu_2\hat{\gamma}^{\alpha} - \mu_3(\hat{\gamma}+\lambda)^{\alpha}\right)\gamma\hat{\beta}\|\mathbf{s}\| \end{aligned} \tag{22}$$

If μ_3 is chosen such that $\mu_3 \geq \mu_2$, the system trajectories are guaranteed to achieve the sliding manifold. Moreover, the Lyapunov inequality remains valid under hard saturation due to the bounded nature of the saturated control input. The proof is completed. □

Remark 2. *The rejection input term* $-\mu_3\hat{\beta}(\hat{\gamma}+\lambda)^{\alpha}\mathbf{s}/\|\mathbf{s}\|$ *serves as an adaptive mechanism to preserve robustness during the transient period, especially before the DOB has fully converged. Beyond this, it also compensates for residual disturbances and mitigates the effects of actuator saturation. By adjusting the exponent* α *the designer can control the rejection intensity to balance chattering suppression and convergence behavior.*

3. Design of Adaptive Sliding Mode-Based DOB

A disturbance observer is developed using a virtual system that replicates the nominal dynamics of the actual plant. By comparing the system's actual behavior with the expected model response, external disturbances and model uncertainties can be effectively estimated and compensated for. A virtual system is constructed as follows.

$$\mathbf{M}_o\dot{\mathbf{z}}+\mathbf{C}_o\mathbf{z}+\mathbf{G}_o \;=\; \mathbf{\Phi}(\boldsymbol{\tau})\cdot\boldsymbol{\tau}+\hat{\mathbf{d}}_l+\boldsymbol{\tau}_v \tag{23}$$

where $\mathbf{z}$ represents the virtual velocity state of the observer and $\boldsymbol{\tau}_v$ is a robust control input that drives the virtual system to the sliding manifold.

To enable disturbance estimation without requiring direct access to acceleration measurements, a first-order virtual system is designed to emulate the velocity dynamics of the actual system, allowing for the residual to be captured through a sliding variable. The sliding manifold is designed as follows.

$$\boldsymbol{\varsigma} \;=\; c(\dot{\mathbf{q}}-\mathbf{z}) \tag{24}$$

where $c>0$ is the gain of the sliding manifold.

According to (4), (23), and (24) we can derive the sliding manifold dynamics.

$$\mathbf{M}_o\dot{\boldsymbol{\varsigma}} \;=\; -\mathbf{C}_o\boldsymbol{\varsigma}+c\tilde{\mathbf{d}}_l-c\boldsymbol{\tau}_v \tag{25}$$

where $\tilde{\mathbf{d}}_l \;=\; \mathbf{d}_l-\hat{\mathbf{d}}_l$.

Let $\beta_1>0$ denote a constant upper bound on the norm of the disturbance estimation error $\tilde{\mathbf{d}}_l$, as specified in Assumption 3 below. Its adaptive estimate is denoted by $\hat{\beta}_1$, and the corresponding estimation error is defined as $\tilde{\beta}_1 \;=\; \beta_1-\hat{\beta}_1$. The virtual control input is chosen as follows.

$$\boldsymbol{\tau}_v \;=\; \mathbf{M}_o\boldsymbol{\varsigma}+\left(\hat{\beta}+\hat{\beta}_1\right)\mathrm{sgn}(\boldsymbol{\varsigma}) \tag{26}$$

where $\hat{\beta}$ is the adaptive estimate obtained by the ICASMC and is incorporated into the observer switching gain to improve the initial estimation transient.

The adaptive law for $\hat{\beta}_1$ is given by

$$\dot{\hat{\beta}}_1 \;=\; k_1\|\boldsymbol{\varsigma}\| \tag{27}$$

where $k_1>0$ is the gain of adaptive law.

To examine the convergence of the observer sliding variable $\boldsymbol{\varsigma}$ governed by (25), we consider the virtual control input in (26) and the adaptive law in (27). The following Lyapunov function candidate is used for this analysis.

$$V_2 \;=\; \frac{1}{2c}\boldsymbol{\varsigma}^T\mathbf{M}_o\boldsymbol{\varsigma}+\frac{1}{2k_1}\tilde{\beta}_1^2 \tag{28}$$

Property 1. *The matrix* $\dot{\mathbf{M}}_o(\mathbf{q})-2\mathbf{C}_o(\mathbf{q},\dot{\mathbf{q}})$ *is skew-symmetric, and satisfies the following identity:*

$$\mathbf{x}^T\left(\dot{\mathbf{M}}_o-2\mathbf{C}_o\right)\mathbf{x} \;=\; 0,\quad \forall\mathbf{x}\in\mathbb{R}^n \tag{29}$$

By applying Property 1, the time derivative of V_2 is obtained as:

$$\begin{aligned}\dot{V}_2 \;&=\; \tfrac{1}{2c}\boldsymbol{\varsigma}^T\dot{\mathbf{M}}_o\boldsymbol{\varsigma}+\tfrac{1}{c}\boldsymbol{\varsigma}^T\mathbf{M}_o\dot{\boldsymbol{\varsigma}}+\tfrac{1}{k_1}\tilde{\beta}_1\dot{\tilde{\beta}}_1\\ &=\; \tfrac{1}{2c}\boldsymbol{\varsigma}^T\dot{\mathbf{M}}_o\boldsymbol{\varsigma}-\tfrac{1}{c}\boldsymbol{\varsigma}^T\mathbf{C}_o\boldsymbol{\varsigma}+\boldsymbol{\varsigma}^T\tilde{\mathbf{d}}_l-\boldsymbol{\varsigma}^T\boldsymbol{\tau}_v-\tfrac{1}{k_1}\beta_1\dot{\hat{\beta}}_1+\tfrac{1}{k_1}\hat{\beta}_1\dot{\hat{\beta}}_1\\ &=\; \boldsymbol{\varsigma}^T\tilde{\mathbf{d}}_l-\boldsymbol{\varsigma}^T\boldsymbol{\tau}_v-\tfrac{1}{k_1}\beta_1\dot{\hat{\beta}}_1+\tfrac{1}{k_1}\hat{\beta}_1\dot{\hat{\beta}}_1\end{aligned} \tag{30}$$

Assumption 3. *The estimated lumped disturbance error $\widetilde{\mathbf{d}}_l$ from the DOB is upper bound by a constant β_1, satisfying the following inequality:*

$$\left\|\widetilde{\mathbf{d}}_l\right\| \leq \beta_1 \tag{31}$$

This assumption is physically justified by the fact that in real-world robotic systems, the control inputs and system states are constrained by hardware limits, such as actuator torque saturation. Since the total energy of the mechanical system remains finite under these physical constraints, the lumped uncertainty and its corresponding estimation error cannot grow indefinitely. This physical reality provides a valid foundation for assuming the boundedness of $\widetilde{\mathbf{d}}_l$ within the stability analysis.

According to Assumption 3, $\boldsymbol{\varsigma}^T\widetilde{\mathbf{d}}_l \leq \|\boldsymbol{\varsigma}\|\left\|\widetilde{\mathbf{d}}_l\right\| \leq \beta_1\|\boldsymbol{\varsigma}\|$ holds, thus the following inequality can be derived.

$$\begin{aligned} \dot{V}_2 &\leq \beta_1\|\boldsymbol{\varsigma}\| - \beta_1\|\boldsymbol{\varsigma}\| + \hat{\beta}_1\|\boldsymbol{\varsigma}\| - \boldsymbol{\varsigma}^T\boldsymbol{\tau}_v \\ &= \hat{\beta}_1\|\boldsymbol{\varsigma}\| - \boldsymbol{\varsigma}^T\mathbf{M}_o\boldsymbol{\varsigma} - \left(\hat{\beta} + \hat{\beta}_1\right)\|\boldsymbol{\varsigma}\| \\ &= -\boldsymbol{\varsigma}^T\mathbf{M}_o\boldsymbol{\varsigma} - \hat{\beta}\|\boldsymbol{\varsigma}\| \\ &\leq 0 \end{aligned} \tag{32}$$

As a result, the virtual system is ensured to converge to the real system under the proposed observer dynamics.

Lemma 1. *Suppose that ideal sliding motion is established and maintained on $\boldsymbol{\varsigma} = 0$. Let $\boldsymbol{\tau}_{v,eq}$ denote the equivalent value of the virtual control input. Then the following component-wise relation holds.*

$$\operatorname{sgn}(\boldsymbol{\tau}_{v,eq}) \;=\; \operatorname{sgn}(\widetilde{\mathbf{d}}_l) \tag{33}$$

Proof. During ideal sliding motion, $\boldsymbol{\varsigma} = 0$ and $\dot{\boldsymbol{\varsigma}} \;=\; 0$. Substituting these conditions into (25), with the virtual input interpreted as its equivalent value, gives

$$\mathbf{0} \;=\; c\widetilde{\mathbf{d}}_l - c\boldsymbol{\tau}_{v,eq} \tag{34}$$

Since $c > 0$, it follows that

$$\boldsymbol{\tau}_{v,eq} \;=\; \widetilde{\mathbf{d}}_l \tag{35}$$

Taking the component-wise sign yields (33). □

Lemma 2. *Let $V(x)$ be a continuously differentiable, positive definite function. Assume that there exist functions $\psi_1(\cdot)$ and $\psi_2(\cdot)$, both strictly increasing and satisfying $\psi_1(0) = \psi_2(0) = 0$, such that:*

$$\psi_1(\|x\|) \leq V(x) \leq \psi_2(\|x\|) \tag{36}$$

And the time derivative of $V(x)$ satisfies

$$\dot{V}(x) \leq -\kappa_1 V(x) + \kappa_2 \tag{37}$$

for some constants $\kappa_1 > 0$, $\kappa_2 > 0$. Then the state $x(t)$ is uniformly bounded for all $t \geq 0$, given that the initial state $x(0)$ is bounded.

Theorem 2. *To enhance observer stability and integrate the controller effectively, an Adaptive Sliding Mode Disturbance Observer (ASMDOB) is proposed.*

$$\begin{cases} \hat{\mathbf{d}}_l \;=\; \delta_1\mathbf{M}_o\boldsymbol{\varsigma} + \boldsymbol{\upsilon} \\ \dot{\boldsymbol{\upsilon}} \;=\; \delta_2\left(\hat{\beta} + \hat{\beta}_1 + \hat{\beta}_2\right)\operatorname{sgn}(\boldsymbol{\tau}_v) \end{cases} \tag{38}$$

Then, the dynamics of the disturbance estimation error $\dot{\widetilde{\mathbf{d}}}_l$ is obtained as follows.

$$\dot{\widetilde{\mathbf{d}}}_l \;=\; \dot{\mathbf{d}}_l - \delta_1\dot{\mathbf{M}}_o\boldsymbol{\varsigma} - \delta_1\mathbf{M}_o\dot{\boldsymbol{\varsigma}} - \delta_2\left(\hat{\beta} + \hat{\beta}_1 + \hat{\beta}_2\right)\operatorname{sgn}(\boldsymbol{\tau}_v) \tag{39}$$

The adaptive law for $\hat{\beta}_2$ is designed as follows:

$$\dot{\hat{\beta}}_2 = k_2\left(\|\boldsymbol{\tau}_v\| - \hat{\beta}_2\right) \tag{40}$$

Proof. Consider the following Lyapunov function

$$V_3 = \frac{1}{2}\tilde{\mathbf{d}}_l^T\tilde{\mathbf{d}}_l + \frac{1}{2k_2}\tilde{\beta}_2^2 \tag{41}$$

The time derivative of V_3 is obtained as follows:

$$\begin{aligned}\dot{V}_3 &= \tilde{\mathbf{d}}_l^T\dot{\tilde{\mathbf{d}}}_l + \tfrac{1}{k_2}\tilde{\beta}_2\dot{\tilde{\beta}}_2 \\ &= \tilde{\mathbf{d}}_l^T\left(\dot{\mathbf{d}}_l - \delta_1\dot{\mathbf{M}}_o\boldsymbol{\varsigma} - \delta_1\mathbf{M}_o\dot{\boldsymbol{\varsigma}} - \delta_2\left(\hat{\beta} + \hat{\beta}_1 + \hat{\beta}_2\right)\mathrm{sgn}(\boldsymbol{\tau}_v)\right) + \tfrac{1}{k_2}\tilde{\beta}_2\dot{\tilde{\beta}}_2\end{aligned} \tag{42}$$

Assumption 4. *There exists a constant β_2 that satisfies the following inequality.*

$$\tilde{\mathbf{d}}_l^T\left(\dot{\mathbf{d}}_l - \delta_1\dot{\mathbf{M}}_o\boldsymbol{\varsigma} - \delta_1\mathbf{M}_o\dot{\boldsymbol{\varsigma}}\right) \le \beta_2\|\boldsymbol{\tau}_v\| \tag{43}$$

Consequently, the following inequality is derived:

$$\begin{aligned}\dot{V}_3 &\le \beta_2\|\boldsymbol{\tau}_v\| + \tfrac{1}{k_2}\tilde{\beta}_2\dot{\tilde{\beta}}_2 - \delta_2\tilde{\mathbf{d}}_l^T\left(\hat{\beta} + \hat{\beta}_1 + \hat{\beta}_2\right)\mathrm{sgn}(\boldsymbol{\tau}_v) \\ &= \beta_2\|\boldsymbol{\tau}_v\| - \beta_2\|\boldsymbol{\tau}_v\| + \beta_2\hat{\beta}_2 + \hat{\beta}_2\|\boldsymbol{\tau}_v\| - \hat{\beta}_2^2 - \delta_2\tilde{\mathbf{d}}_l^T\left(\hat{\beta} + \hat{\beta}_1 + \hat{\beta}_2\right)\mathrm{sgn}(\boldsymbol{\tau}_v)\end{aligned} \tag{44}$$

Under the ideal-sliding conditions of Lemma 1, the equivalent virtual input satisfies $\boldsymbol{\tau}_{v,eq} = \tilde{\mathbf{d}}_l$. Furthermore, assume that the disturbance estimation error satisfies $\left\|\tilde{\mathbf{d}}_l\right\| \le \hat{\beta} + \hat{\beta}_1$. Then, the following inequality holds: $-\left(\hat{\beta} + \hat{\beta}_1\right)\left\|\tilde{\mathbf{d}}_l\right\| \le -\left\|\tilde{\mathbf{d}}_l\right\|^2$. Let $\varepsilon_0 \triangleq \tilde{\beta}_2\beta_2$, which vanishes asymptotically as the adaptation of β_2 proceeds.

$$\begin{aligned}\dot{V}_3 &= \beta_2\hat{\beta}_2 - \hat{\beta}_2^2 - \left(\hat{\beta} + \hat{\beta}_1\right)\left\|\tilde{\mathbf{d}}_l\right\| \\ &\le -\left\|\tilde{\mathbf{d}}_l\right\|^2 + \beta_2\hat{\beta}_2 - \hat{\beta}_2^2 \\ &= -2\delta V_3 + \varepsilon_0\end{aligned} \tag{45}$$

Hence, by invoking Lemma 2 along with the exponential convergence property of the Lyapunov function, it follows that the proposed ASMDOB achieves exponential convergence of the estimation error, which in turn ensures the robust stability of the closed-loop system under uncertainties and actuator saturation constraints. □

Remark 3. *The adaptive estimate $\hat{\beta}$, obtained by the ICASMC to compensate for uncertainties and actuator saturation, is also used in the ASMDOB switching gain to improve transient performance during the initial convergence phase. By incorporating this adaptive term, the proposed observer achieves faster and more stable disturbance estimation. Moreover, the reuse of $\hat{\beta}$ contributes to structural consistency between the controller and the observer, while also reducing the need for conservative initial gain tuning.*

Remark 4. *The sliding variable $\boldsymbol{\varsigma}$ is a velocity-level residual between the measured motion and the virtual system. When a disturbance acts, this residual responds immediately, using it as a lead input to the observer reduce phase lag and shortens the initial estimation latency. The added term $\delta_1\mathbf{M}_o\boldsymbol{\varsigma}$ performs this role: pre-multiplication by the nominal inertia $\mathbf{M}_o$ and δ_1 maps the residual to the torque scale, and $\delta_1 > 0$ is a tuning gain that sets the observer's effective bandwidth. Larger δ_1 yields faster transients but increases sensitivity to velocity-measurement noise, smaller values trade speed for smoothness.*

Remark 5. *The proposed ASMDOB incorporates the adaptive estimate $\hat{\beta}$ obtained by the ICASMC to improve transient performance during the initial convergence phase. By adaptively initializing the observer gain, this approach removes the need for conservative initial assumptions on DOB parameters, thereby enabling faster disturbance rejection without sacrificing robustness.*

4. Numerical Simulations and Experiments

The effectiveness of the proposed controller and DOB was evaluated through numerical simulation and experimental validation, both conducted using MATLAB/Simulink R2024b.

4.1. Numerical Simulation

The effectiveness of the proposed integrated controller (ICASMC + ASMDOB) was validated through numerical simulation.

We consider a planar spacecraft with a 2-DOF manipulator (Figure 2, Table 2), whose dynamics are described by the following equation:

$$\mathbf{M}\ddot{\mathbf{q}} + \mathbf{C}\dot{\mathbf{q}} = \mathbf{u} + \mathbf{d}_l \tag{46}$$

where the generalized-coordinate vector $\mathbf{q}$ is defined as $\mathbf{q} = [x_b,\ y_b,\ \theta,\ q_1,\ q_2]^T$. Implementation gains are summarized in Table 3.

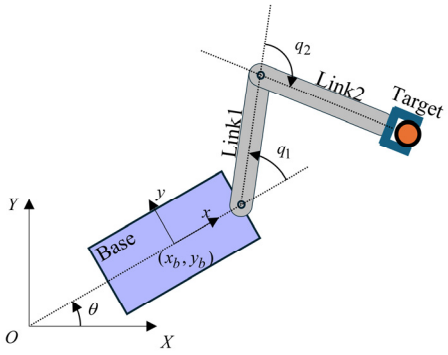


Figure 2. Planar spacecraft with a 2-DOF manipulator, showing base pose (x_b,y_b,θ) and joint angles q_1 and q_2. The physical parameters and actuator limits used in the simulation are listed in Table 2.

Table 2. Parameters of Spacecraft and 2-Link Manipulator.

Component	Mass (kg)	Inertia (kg·m^2)	Length (m)	Actuator Constraints
Base	50.00	5.21	1.00 × 0.50	$F_{b,\max} = 800$ N $\tau_{b,\max} = 500$ N·m
Link1	7.00	0.78	1.00	$\tau_{m,1} = 200$ N·m
Link2 + target	10.00	1.11	1.00	$\tau_{m,2} = 200$ N·m

The gravity term is omitted from (46) because the planar free-floating spacecraft–manipulator model neglects gravitational and gravity-gradient effects. This idealization is specific to the spacecraft simulation and does not apply to the ground-based manipulator experiments.

Table 3. Parameters for ICASMC and ASMDOB.

Module	Parameters
ICASMC	$\mathbf{\Lambda} = diag([30, 30, 37.5, 22.5, 7.5])$ $\boldsymbol{\sigma} = diag([200, 200, 280, 400, 240])$ $\mu_1 = 2,\ \mu_2 = 5,\ \mu_3 = 10,\ \alpha = 5,\ \lambda = 0.0001$
ASMDOB	$c = 8,\ k_1 = 3,\ \delta_1 = 8,\ \delta_2 = 20$
Initial condition	$\mathbf{q}(0) = [5,\ -3, 0, 0.2,\ -0.3]^T$, $\dot{\mathbf{q}}(0) = [0,\ 0,\ 0,\ 0,\ 0]^T$

The desired trajectories were set as follows:

$$\mathbf{q}_d(t) = \begin{bmatrix} 10\cos(0.5t) \\ 7\sin(0.5t) \\ \text{atan2}(3.5\cos(0.5t), -5\sin(0.5t)) \\ \sin(0.2\pi t) + \cos(0.5\pi t) \\ \cos(\pi t) \end{bmatrix} \tag{47}$$

To evaluate the robustness of the proposed controller under extreme operational conditions, the system was subjected to a composite disturbance consisting of both step and sinusoidal components.

Figure 3 shows the generalized coordinate tracking errors. The proposed ICASMC + ASMDOB achieves rapid error decay and near-zero steady-state error, ensuring closed-loop stability under disturbances and input constraints, even in the presence of actuator saturation.

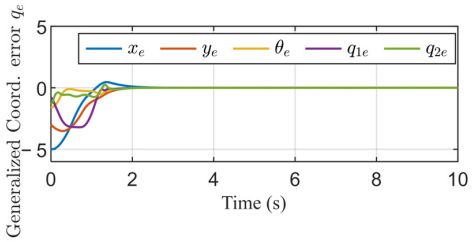


Figure 3. Generalized-coordinate tracking errors in the planar spacecraft–manipulator simulation using the proposed ICASMC–ASMDOB. The curves show the base translational and rotational errors and the manipulator joint-angle errors.

Figure 4 plots the base body thrusts and joint torques together with their limits. The proposed controller respects actuator bounds throughout the maneuver, demonstrating explicit saturation handling.

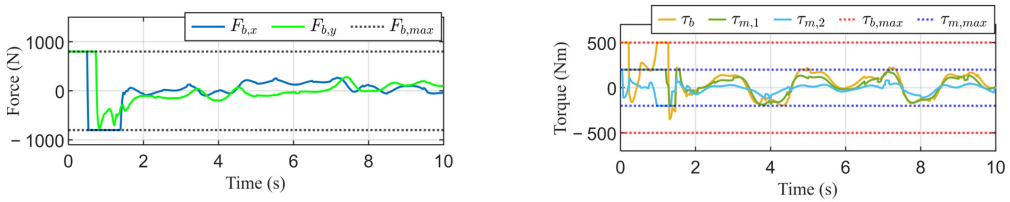


Figure 4. Control inputs and actuator limits: (**a**) Base thrust forces (N); (**b**) base and joint torques (N·m).

The time histories of $\hat{\beta}$ and $\hat{\gamma}$ are shown in Figure 5. Both parameters converge smoothly, indicating a well-conditioned adaptation process.

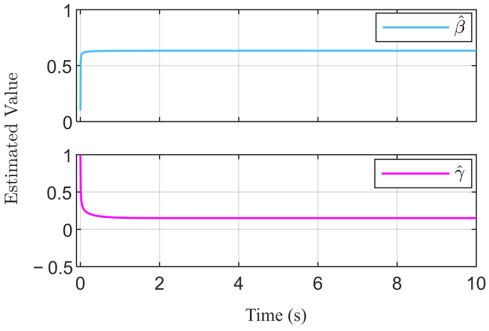


Figure 5. Adaptive parameter estimates of $\hat{\beta}$ and $\hat{\gamma}$ in the simulation.

Figure 6 compares the true lumped disturbances with the estimates from ASMDOB. The close match during both step-like and harmonic disturbances validates the rapid transient response of the proposed observer.

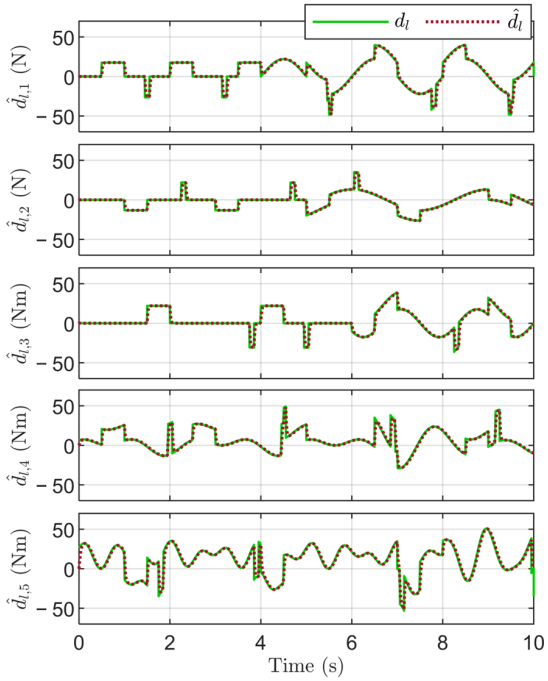


Figure 6. Comparison of actual and estimated lumped disturbances using the proposed ASMDOB.

4.2. Experimental Results

Experiments were conducted using a 3-DOF manipulator shown in Figure 7, equipped with MyActuator-X6 motors (Suzhou Micro Actuator Technology Co., Ltd., Kunshan, China). The controller was implemented on a Teensy 4.1 development board (PJRC.COM, LLC., Sherwood, OR, USA) and operated at 500 Hz, with communication to the motors via CAN bus.

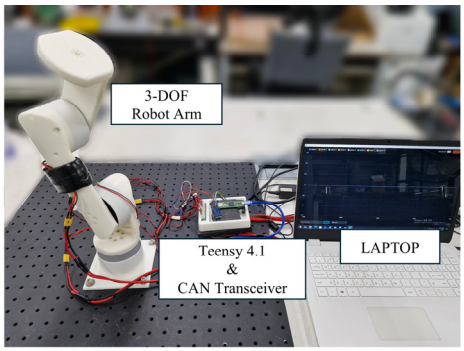


Figure 7. Experimental setup of the 3-DOF robotic manipulator and control hardware.

Unlike the free-floating spacecraft model used in the simulation, the experimental manipulator has a fixed base and is subject to gravity, joint friction, and actuator dynamics. These effects can alter the torque required for tracking and the actuator response, thereby influencing transient tracking errors and saturation behavior. The simulation evaluates the controller under coupled spacecraft–manipulator dynamics, whereas the experiment evaluates its implementation on a physical manipulator. The simulation and the experiment therefore provide complementary validations rather than a direct quantitative comparison. Because the two platforms differ in plant dynamics, actuator limits, and reference

trajectories, numerical differences between them cannot isolate the effects of unmodeled factors such as friction or actuator dynamics. Instead, the experimental comparison quantifies the saturation behavior and tracking performance of the controllers under identical experimental hardware conditions.

The trajectory $q_{d,i}(t) = A_i \sin(3t + \pi)$, $i = 1,2,3$ with $\mathbf{A} = [1.0,1.0,1.5]$ rad was applied to challenge actuator limits. The controller is formulated for an n-DOF system, although further validation is required for higher-DOF manipulators.

Figure 8 compares the joint trajectories obtained with the proposed controller, an SMC comparator with a nonlinear sliding surface, and a PID controller. The SMC comparator combines a model-based equivalent torque with a power-law reaching term. Its sliding variable includes the velocity error, a linear position-error term, and a sign-preserving power of the position error. The control input of the sliding-mode comparator is given by $\mathbf{u}_N = \boldsymbol{\tau}_{N,eq} - \mathbf{K}_N|\mathbf{s}|^{\beta_N}\mathrm{sgn}(\mathbf{s})$, where the equivalent term $\boldsymbol{\tau}_{N,eq}$ is generated using the nonlinear sliding surface $\mathbf{s} = \dot{\mathbf{e}} + \boldsymbol{\Lambda}_N\mathbf{e} + \boldsymbol{\Gamma}_N|\mathbf{e}|^{\alpha_N}\mathrm{sgn}(\mathbf{e})$. The controller parameters for each method are summarized in Table 4.

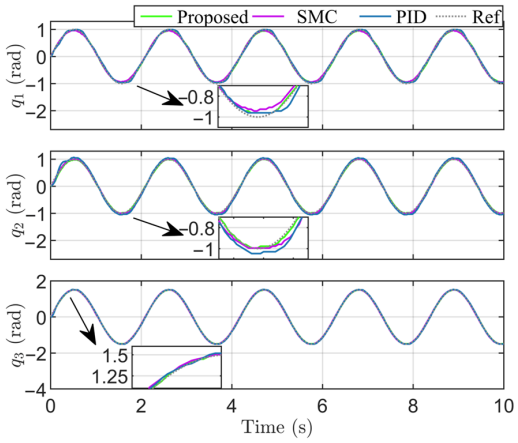


Figure 8. Joint trajectory tracking results of the proposed, SMC, and PID controllers.

Table 4. Parameters for Proposed and Comparators.

Controllers	Parameters
Proposed	$\boldsymbol{\Lambda} = diag([35,11,27])$, $\boldsymbol{\sigma} = diag([0.065,0.19,0.048])$, $\mu_1 = 1.1$, $\mu_2 = 17$, $\mu_3 = 25$, $\alpha = 1.05$, $\lambda = 0.015$ $c = 0.25$, $k_1 = 1$, $k_2 = 1$, $\delta_1 = 0.05$, $\delta_2 = 0.40$
SMC	$\alpha_N = 1.2$, $\beta_N = 0.95$, $\boldsymbol{\Lambda}_N = diag([12,32,17])$, $\boldsymbol{\Gamma}_N = diag([7,9,7])$, $\mathbf{K}_N = diag([0.08,0.17,0.08])$
PID	$\mathbf{K}_p = diag([2.2,6,2.2])$, $\mathbf{K}_i = diag([0.01,0.05,0.01])$, $\mathbf{K}_d = diag([0.05,0.15,0.05])$

For the SMC comparator, α_N is the exponent of the nonlinear position-error term, while β_N is the exponent of the reaching term. The matrices $\boldsymbol{\Lambda}_N$ and $\boldsymbol{\Gamma}_N$ determine the linear and nonlinear components of the sliding variable, respectively, and $\mathbf{K}_N$ determines the reaching gain. Their numerical values are listed in Table 4.

The parameters of the PID controller and the SMC comparator were tuned to reduce tracking errors and excessive control-input fluctuations under the same actuator limits. A zoomed-in view (highlighted in Figure 8) shows the sections where the reference undergoes sharp directional changes, inducing high structural loading and actuator saturation.

Figure 9 presents the actuator torques. The proposed method maintains smooth inputs comparable to PID, excluding slight initial chattering. Under the tested conditions, the SMC comparator exhibits pronounced control-input fluctuations and saturation, particularly in Joint 2. Figure 10 shows the estimated parameters $\hat{\beta}$ and $\hat{\gamma}$, both converging to steady values, indicating stable and effective adaptation.

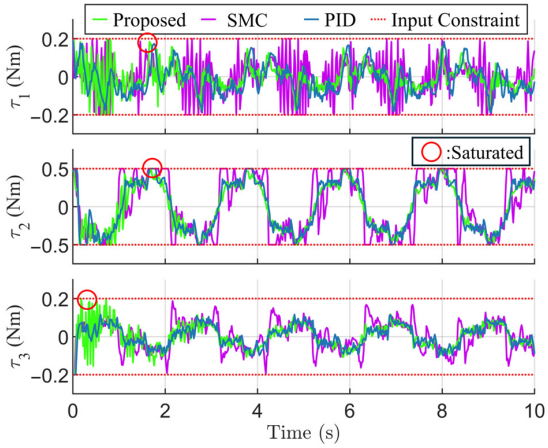


Figure 9. Joint control torques and actuator limits for the proposed, SMC, and PID controllers.

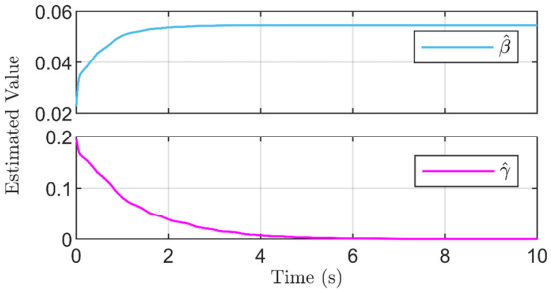


Figure 10. Adaptive parameter estimates of $\hat{\beta}$ and $\hat{\gamma}$ in the experiment.

Figure 11 presents the joint-wise lumped disturbance estimates generated by the ASMDOB during trajectory tracking. Figure 12 compares the tracking errors and total RMSEs. Table 5 summarizes the saturation behavior and tracking performance of the three controllers.

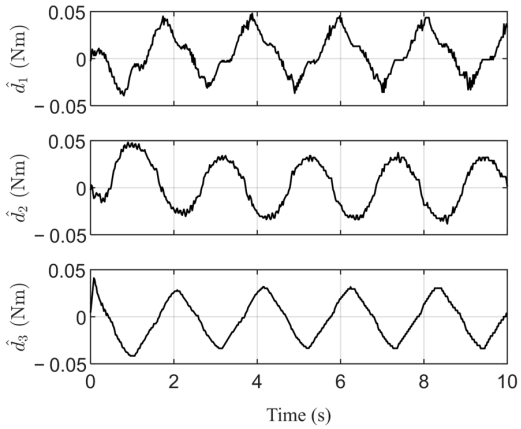


Figure 11. Lumped disturbance estimates for the manipulator joints obtained using the proposed ASMDOB.

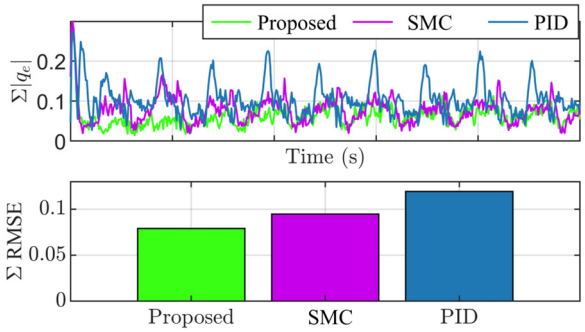


Figure 12. Experimental tracking-error comparison of the proposed ICASMC–ASMDOB, SMC, and PID controllers. The **upper panel** shows the sum of absolute joint tracking errors, and the **lower panel** shows the sum of the joint-wise root-mean-square errors (RMSEs).

Table 5. Quantitative comparison of saturation behavior and tracking performance in the experiments.

Metric	Proposed	SMC	PID
Saturation duration (s)	0.56 (1.9%)	3.80 (12.6%)	1.12 (3.7%)
Saturation count	18	83	11
Saturation after 1 s (s)	0.10	3.42	0.78
Total RMSE (rad)	0.079	0.095	0.119

Table 5 summarizes the saturation behavior and tracking performance of the three controllers. To preserve real-time control performance at 500 Hz, data were logged at 50 Hz; hence, the saturation duration has a resolution of 0.02 s, and a sample was regarded as saturated when $|\tau_i| \geq 0.999\tau_mi$. The proposed controller achieves the shortest cumulative saturation duration of 0.56 s, compared with 3.80 s for SMC and 1.12 s for PID. It also yields the lowest total RMSE of 0.079 rad, compared with 0.095 rad and 0.119 rad, respectively. Thus, under the tested conditions, the shorter saturation duration is accompanied by improved tracking accuracy.

The saturation counts are 18, 83, and 11 for the proposed, SMC, and PID controllers, respectively. Although the proposed controller has a higher count than PID, its cumulative saturation duration is shorter. In addition, the saturation duration after the first second is 0.10 s, compared with 3.42 s for SMC and 0.78 s for PID, indicating that most saturation events of the proposed controller occurred during the initial transient before the adaptive gains and the ASMDOB converged.

5. Discussion and Conclusions

This paper proposed an integrated adaptive robust control framework that combines an Input-Constrained Adaptive Sliding Mode Controller (ICASMC) with an Adaptive Sliding Mode Disturbance Observer (ASMDOB) for robotic manipulators subject to actuator saturation, model uncertainties, and external disturbances. In particular, the uncertainty-bound information estimated by the ICASMC is incorporated into the ASMDOB switching gain, improving the observer transient response while reducing the need for conservative gain selection. The ICASMC further accounts explicitly for actuator saturation and provides adaptive compensation for unknown uncertainties without requiring a priori knowledge of their exact bounds.

The stability properties of the proposed framework were established through Lyapunov-based analysis. The analysis demonstrated the boundedness of the closed-loop signals under actuator saturation and the convergence of the sliding variable toward the sliding manifold. In addition, the proposed ASMDOB guarantees bounded and convergent distur-

bance estimation errors under the stated assumptions. Numerical simulations of a planar spacecraft–manipulator system demonstrated rapid tracking-error reduction, compliance with the prescribed actuator limits, and effective estimation of composite disturbances containing both step-like and sinusoidal components. Experimental validation using a 3-DOF robotic manipulator further showed that the proposed ICASMC–ASMDOB achieves lower tracking errors while maintaining smooth control inputs under the same actuator constraints compared with the SMC comparator and the PID controller. The experimental comparison is limited to these two implemented comparison controllers. These results therefore do not establish comparative performance against other adaptive control methods or isolate the contribution of adaptive information sharing through a separate ablation study. The reported results support the effectiveness of the integrated controller–observer framework under the tested conditions.

The present experimental validation was limited to a 3-DOF rigid-link manipulator with fixed actuator constraints. Future work will therefore investigate the extension of the proposed framework to higher-DOF and flexible-link manipulators, where stronger dynamic coupling, elastic deformation, and vibration modes must be considered. In addition, actuator degradation, faults, and time-varying input constraints will be incorporated to develop fault-tolerant and health-aware extensions of the proposed control framework for safety-critical robotic and space manipulation applications.

Author Contributions: Conceptualization, S.L. and J.K.; methodology, S.L.; software, S.L.; validation, S.L.; formal analysis, S.L. and Y.H.; investigation, S.L.; resources, J.K.; data curation, S.L.; writing—original draft preparation, S.L. and Y.H.; writing—review and editing, S.L., Y.H. and J.K.; visualization, S.L.; supervision, J.K.; project administration, J.K.; funding acquisition, J.K. All authors have read and agreed to the published version of the manuscript.

Funding: This work was supported by the MSIT (Ministry of Science and ICT), Korea, under the National Program for Excellence in SW, supervised by the IITP (Institute of Information & Communications Technology Planning & Evaluation) in 2025 (2022-0-01127). This work was supported by INHA University Research Grant (INHA-77863-1).

Institutional Review Board Statement: Not applicable.

Informed Consent Statement: Not applicable.

Data Availability Statement: Data will be made available on request.

Conflicts of Interest: The authors declare no conflicts of interest.

Appendix A

The main symbols and abbreviations used in this paper are summarized below. A hat denotes an estimated quantity, a tilde denotes the corresponding estimation error, and a dot denotes differentiation with respect to time.

Table A1. Main symbols.

Symbol	Description
n	Number of coordinates in the system model
$\mathbf{q}$, $\dot{\mathbf{q}}$, $\ddot{\mathbf{q}}$	Position, velocity, and acceleration vectors
$\mathbf{q}_d$, $\dot{\mathbf{q}}_d$, $\ddot{\mathbf{q}}_d$	Desired position, velocity, and acceleration vectors
$\mathbf{q}_e$	Tracking error, defined as $\mathbf{q} - \mathbf{q}_d$
$\mathbf{M}_o$, $\mathbf{C}_o$, $\mathbf{G}_o$	Nominal inertia matrix, Coriolis matrix, and gravity vector
$\mathbf{d}_l$	Lumped disturbance, including model uncertainties and external disturbances

Table A1. *Cont.*

Symbol	Description
$\hat{\mathbf{d}}_l$, $\tilde{\mathbf{d}}_l$	Disturbance estimate and estimation error, with $\tilde{\mathbf{d}}_l = \mathbf{d}_l - \hat{\mathbf{d}}_l$
$\boldsymbol{\tau}$, $\mathbf{u}$	Commanded input and input after actuator saturation
τ_{mi}	Input limit of actuator i
$\boldsymbol{\Phi}(\tau_i)$, $\mathbf{f}(\tau_i)$	Diagonal saturation matrix and its ith diagonal entry
$\mathbf{s}$	Controller sliding variable, defined as $\dot{\mathbf{q}}_e + \boldsymbol{\Lambda}\mathbf{q}_e$
$\boldsymbol{\Lambda}$	Positive definite diagonal matrix defining the controller sliding variable
$\boldsymbol{\tau}_{eq}$, $\boldsymbol{\tau}_r$	Equivalent and rejection components of the commanded input
$\mathbf{H}_{eq}$, $\hat{\mathbf{H}}_{eq}$	Equivalent term defined in the controller derivation and its estimated counterpart
β	Constant characterizing the uncertainty bound in Assumption 2
γ	Positive lower bound on the saturation factors assumed in Assumption 1
$\hat{\beta}$, $\hat{\gamma}$	Adaptive parameter estimates used by the ICASMC
$\tilde{\beta}$, $\tilde{\gamma}$	Estimation errors, defined as $\beta - \hat{\beta}$ and $\gamma - \hat{\gamma}$
μ_1, μ_2	Gains in the ICASMC adaptive laws
μ_3, $\boldsymbol{\sigma}$, λ, α	Gain parameters and exponent used in the rejection input
$\mathbf{z}$	Virtual velocity state
$\boldsymbol{\varsigma}$	Observer sliding variable, defined as $c(\dot{\mathbf{q}} - \mathbf{z})$
c	Positive scaling gain of the observer sliding variable
$\boldsymbol{\tau}_v$	Virtual control input
$\boldsymbol{\tau}_{v,eq}$	Equivalent virtual control input during ideal sliding motion
β_1, $\hat{\beta}_1$, $\tilde{\beta}_1$	Disturbance-estimation-error bound in Assumption 3, its adaptive estimate, and the associated estimation error
β_2, $\hat{\beta}_2$, $\tilde{\beta}_2$	Bounding constant in Assumption 4, its adaptive estimate, and the associated estimation error
k_1, k_2	Gains in the observer adaptive laws
δ_1, δ_2	Gains in the disturbance-observer update
V_1, V_2, V_3	Lyapunov function candidates used in the controller and observer analyses
$\boldsymbol{\Lambda}_N$, $\boldsymbol{\Gamma}_N$, $\mathbf{K}_N$	Gain matrices of the SMC comparator
α_N, β_N	Exponents in the comparator sliding variable and reaching term of the SMC comparator
$\mathbf{K}_p$, $\mathbf{K}_i$, $\mathbf{K}_d$	Proportional, integral, and derivative gain matrices of the PID controller

Table A2. Abbreviations.

Abbreviation	Full Term
DOF	Degree of freedom
SMC	Sliding mode control
ASMC	Adaptive sliding mode control
ICASMC	Input-Constrained Adaptive Sliding Mode Controller
DOB	Disturbance Observer
ASMDOB	Adaptive Sliding Mode Disturbance Observer
PID	Proportional–integral–derivative
MPC	Model Predictive Control
ETC	Event-triggered control
BLF	Barrier Lyapunov Function
RMSE	Root-mean-square error
CAN	Controller Area Network
UAV	Unmanned aerial vehicle

References

1. Shao, K.; Zheng, J.; Tang, R.; Li, X.; Man, Z.; Liang, B. Barrier function-based adaptive sliding mode control for uncertain systems with input saturation. *IEEE/ASME Trans. Mechatron.* **2022**, *27*, 4258–4268. [CrossRef]
2. Xiao, B.; Hu, Q.; Zhang, Y. Adaptive sliding mode fault-tolerant attitude tracking control for flexible spacecraft under actuator saturation. *IEEE Trans. Control Syst. Technol.* **2011**, *20*, 1605–1612. [CrossRef]
3. Hu, Y.; Yan, H.; Zhang, H.; Wang, M.; Zeng, L. Robust adaptive fixed-time sliding-mode control for uncertain robotic systems with input saturation. *IEEE Trans. Cybern.* **2022**, *53*, 2636–2646. [CrossRef] [PubMed]

4. Islam, S.; Liu, X.P. Robust sliding mode control for robot manipulators. *IEEE Trans. Ind. Electron.* **2010**, *58*, 2444–2453. [CrossRef]
5. Seo, D.; Kang, J. Controller design for active four-wheel steering and four-wheel independent drive-based mobile robot: Enhancing cornering performance in negative phase. *Int. J. Control Autom. Syst.* **2025**, *23*, 235–248. [CrossRef]
6. Kim, K.; Seo, D.; An, C.; Kong, D.; Kang, J. Torque vectoring control of in-wheel motor driven trailer for lateral stability of trailer. *Veh. Syst. Dyn.* **2026**, *64*, 457–478. [CrossRef]
7. Baek, J.; Jin, M.; Han, S. A new adaptive sliding-mode control scheme for application to robot manipulators. *IEEE Trans. Ind. Electron.* **2016**, *63*, 3628–3637. [CrossRef]
8. Bae, J.; Kang, J. Design concepts and control algorithm to minimize the control effort for earth-orbit-raising solar sails. *Aerosp. Sci. Technol.* **2024**, *146*, 108994. [CrossRef]
9. Liang, J.; Chen, Y.; Lai, N.; He, B.; Miao, Z.; Wang, Y. Low-complexity prescribed performance control for unmanned aerial manipulator robot system under model uncertainty and unknown disturbances. *IEEE Trans. Ind. Inform.* **2021**, *18*, 4632–4641. [CrossRef]
10. Ma, H.; Zhou, Q.; Li, H.; Lu, R. Adaptive prescribed performance control of a flexible-joint robotic manipulator with dynamic uncertainties. *IEEE Trans. Cybern.* **2021**, *52*, 12905–12915. [CrossRef] [PubMed]
11. Yang, C.; Fang, Z.; Ren, H.; Lu, W.; Xia, Y. Interval uncertainty-oriented impedance force control for space manipulator with time-dependent reliability. *Acta Astronaut.* **2024**, *222*, 207–218. [CrossRef]
12. He, W.; Kang, F.; Kong, L.; Feng, Y.; Cheng, G.; Sun, C. Vibration control of a constrained two-link flexible robotic manipulator with fixed-time convergence. *IEEE Trans. Cybern.* **2021**, *52*, 5973–5983. [CrossRef] [PubMed]
13. Shao, X.; Sun, G.; Yao, W.; Liu, J.; Wu, L. Adaptive sliding mode control for quadrotor UAVs with input saturation. *IEEE/ASME Trans. Mechatron.* **2021**, *27*, 1498–1509. [CrossRef]
14. Zhang, J.; Zhang, S.; Lin, P. Event-triggered model predictive control of positive systems with random actuator saturation. *Nonlinear Dyn.* **2021**, *105*, 417–437. [CrossRef] [PubMed]
15. Zhu, G.; Ma, Y.; Hu, S. Event-triggered adaptive PID fault-tolerant control of underactuated ASVs under saturation constraint. *IEEE Trans. Syst. Man Cybern. Syst.* **2023**, *53*, 4922–4933. [CrossRef]
16. Forouzanfar, M.; Gagliardi, G.; Tedesco, F.; Casavola, A. Integrated model-based control allocation strategies oriented to predictive maintenance of saturated actuators. *IEEE Trans. Autom. Sci. Eng.* **2024**, *22*, 1045–1056. [CrossRef]
17. Zhai, M.; Sun, N.; Yang, T.; Fang, Y. Underactuated mechanical systems with both actuator and actuated/unactuated state constraints: A predictive control-based approach. *IEEE/ASME Trans. Mechatron.* **2022**, *28*, 1359–1371. [CrossRef]
18. Cruz-Ortiz, D.; Chairez, I.; Poznyak, A. Sliding-mode control of full-state constraint nonlinear systems: A barrier Lyapunov function approach. *IEEE Trans. Syst. Man Cybern. Syst.* **2022**, *52*, 6593–6606. [CrossRef]
19. Niu, B.; Zhao, J. Barrier Lyapunov functions for the output tracking control of constrained nonlinear switched systems. *Syst. Control Lett.* **2013**, *62*, 963–971. [CrossRef]
20. Zhao, K.; Song, Y.; Chen, C.P.; Chen, L. Control of nonlinear systems under dynamic constraints: A unified barrier function-based approach. *Automatica* **2020**, *119*, 109102. [CrossRef]
21. Zhu, Z.; Xia, Y.; Fu, M. Adaptive sliding mode control for attitude stabilization with actuator saturation. *IEEE Trans. Ind. Electron.* **2011**, *58*, 4898–4907. [CrossRef]
22. Sariyildiz, E.; Oboe, R.; Ohnishi, K. Disturbance observer-based robust control and its applications: 35th anniversary overview. *IEEE Trans. Ind. Electron.* **2019**, *67*, 2042–2053. [CrossRef]
23. Sariyildiz, E.; Hangai, S.; Uzunovic, T.; Nozaki, T.; Ohnishi, K. Stability and robustness of the disturbance observer-based motion control systems in discrete-time domain. *IEEE/ASME Trans. Mechatron.* **2020**, *26*, 2139–2150. [CrossRef]
24. Zhu, Y.; Qiao, J.; Guo, L. Adaptive sliding mode disturbance observer-based composite control with prescribed performance of space manipulators for target capturing. *IEEE Trans. Ind. Electron.* **2018**, *66*, 1973–1983. [CrossRef]
25. Xi, R.-D.; Xiao, X.; Ma, T.-N.; Yang, Z.-X. Adaptive sliding mode disturbance observer based robust control for robot manipulators towards assembly assistance. *IEEE Robot. Autom. Lett.* **2022**, *7*, 6139–6146. [CrossRef]
26. Wen, C.; Zhou, J.; Liu, Z.; Su, H. Robust adaptive control of uncertain nonlinear systems in the presence of input saturation and external disturbance. *IEEE Trans. Autom. Control* **2011**, *56*, 1672–1678. [CrossRef]
27. Sai, H.; Xu, Z.; He, S.; Zhang, E.; Zhu, L. Adaptive nonsingular fixed-time sliding mode control for uncertain robotic manipulators under actuator saturation. *ISA Trans.* **2022**, *123*, 46–60. [CrossRef] [PubMed]
28. Wu, Y.; Huang, R.; Wang, Y.; Wang, J. Adaptive tracking control of robot manipulators with input saturation and time-varying output constraints. *Asian J. Control* **2021**, *23*, 1476–1489. [CrossRef]
29. Yao, Q. Adaptive trajectory tracking control of a free-flying space manipulator with guaranteed prescribed performance and actuator saturation. *Acta Astronaut.* **2021**, *185*, 283–298. [CrossRef]
30. Sun, W.; Wu, Y.; Lv, X. Adaptive neural network control for full-state constrained robotic manipulator with actuator saturation and time-varying delays. *IEEE Trans. Neural Netw. Learn. Syst.* **2021**, *33*, 3331–3342. [CrossRef] [PubMed]

31. Sun, Y.; Liu, J.; Gao, Y.; Liu, Z.; Zhao, Y. Adaptive neural tracking control for manipulators with prescribed performance under input saturation. *IEEE/ASME Trans. Mechatron.* **2022**, *28*, 1037–1046. [CrossRef]
32. Liu, K.; Yang, P.; Jiao, L.; Wang, R.; Yuan, Z.; Li, T. Observer-based adaptive finite-time neural control for constrained nonlinear systems with actuator saturation compensation. *IEEE Trans. Instrum. Meas.* **2024**, *73*, 7502516. [CrossRef]
33. Li, Y.; Zhang, J.; Liu, W.; Tong, S. Observer-based adaptive optimized control for stochastic nonlinear systems with input and state constraints. *IEEE Trans. Neural Netw. Learn. Syst.* **2021**, *33*, 7791–7805. [CrossRef] [PubMed]
34. Pan, H.; Sun, W.; Gao, H.; Jing, X. Disturbance observer-based adaptive tracking control with actuator saturation and its application. *IEEE Trans. Autom. Sci. Eng.* **2015**, *13*, 868–875. [CrossRef]
35. Hu, Q. Robust adaptive sliding mode attitude maneuvering and vibration damping of three-axis-stabilized flexible spacecraft with actuator saturation limits. *Nonlinear Dyn.* **2009**, *55*, 301–321. [CrossRef]

Disclaimer/Publisher's Note: The statements, opinions and data contained in all publications are solely those of the individual author(s) and contributor(s) and not of MDPI and/or the editor(s). MDPI and/or the editor(s) disclaim responsibility for any injury to people or property resulting from any ideas, methods, instructions or products referred to in the content.